Supplementary Material

Deriving Cool Flame Propagation Speeds by Means of an Ozone-Seeded, Stagnation Plate Burner Configuration

Thomas Panaget[a,b,e], Pierre Bragança[c], Bertrand Lecordier[d], Amaury Lahccen[e], Christophe Cuvier[c], Sébastien Batut[e], Yann Fenard[e], Guillaume Vanhove[e] and Laure Pillier[e,*]

[a] *Univ. Lille, Inserm, CHU Lille, Institut Pasteur Lille, U1167 – RID-AGE – Facteurs de risque et déterminants moléculaires des maladies liées au vieillissement, F-59000 Lille, France*

[b] *Junia, Health and Environment, Laboratory of Sustainable Chemistry and Health, F-59000 Lille, France*

[c] *Univ. Lille, CNRS, ONERA, Arts et Métiers Institute of Technology, Centrale Lille, UMR 9014 - LMFL - Laboratoire de Mécanique des Fluides de Lille - Kampé de Fériet, F-59000 Lille, France*

[d] *Normandie Univ., UNIROUEN, INSA Rouen, CNRS, CORIA, 76000 Rouen, France*

[e] *Univ. Lille, CNRS, UMR 8522 - PC2A - Physicochimie des Processus de Combustion et de l'Atmosphère, F-59000 Lille, France*

Figure S1. Direct comparison between the conventional PIV image processing and the image processing developed in this study. Both flames conditions are $\phi = 0.4$, $x_{O3} = 1.9\%$, with inlet velocities respectively equal to 0.75 $m.s^{-1}$ and 1.10 $m.s^{-1}$.

Figure S2. Evolution of the standard deviation on the determination of the reference axial velocity $S_{u,ref}$ depending on the number of grid points used in the simulation of the axial velocity profile. Simulations are performed with the O_3-submechanism from Jian et al [1].

Figure S3. Experimental (open diamonds) PIV measurement of the axial velocity profile for the cool flame at $\phi = 0.5$, $x_{O3} = 1.5\%$, and simulated (continuous lines) profiles with different domain sizes *l*. Simulations are performed with the O_3-submechanism from Jian et al [1].

Figure S4. Evolution of the standard deviation on the determination of the value of $S_{u,ref}$ (a) and its position (b) depending on the size of the simulated domain. Simulations are performed with the O_3-submechanism from Jian et al [1].

Figure S5. Comparison between experimental axial velocity profiles measured by PIV (□) and simulated ones with different O_3 submechanisms, respectively from Jian et al. [1], Halter et al. [2] and Zhao et al. [3], for the cool flame at $\phi = 0.4$, $x_{O3} = 1.7\%$, at different strain rates.

Figure S6. Comparison between experimental axial velocity profiles measured by PIV (□) and simulated ones with different O_3 submechanisms, respectively from Jian et al. [1], Halter et al. [2] and Zhao et al. [3], for the cool flame at $\phi = 0.4$, $x_{O3} = 1.9\%$, at different strain rates.

Figure S7. Comparison between experimental axial velocity profiles measured by PIV (□) and simulated ones with different O_3 submechanisms, respectively from Jian et al. [1], Halter et al. [2] and Zhao et al. [3], for the cool flame at $\phi = 0.45$, $x_{O3} = 1.7\%$, at different strain rates.

Figure S8. Comparison between simulated axial velocity profiles with O_3-submechanism from Jian et al. [1] and from Jian et al. with O_3+M reactions from Halter et al. [2], for the cool flame at $\phi = 0.5$, $x_{O3} = 1.5\%$ and strain rate of 127 s^{-1}.

Table T1 : Cool flame conditions

Table T2. Reactions and rate constant parameters for the three O_3-submechanisms used in the current study

Figure S1. Direct comparison between the conventional PIV image processing and the image processing developed in this study. Both flames conditions are $\phi = 0.4$, $x_{O3} = 1.9\%$, with inlet velocities respectively equal to 0.75 $m.s^{-1}$ and 1.10 $m.s^{-1}$.

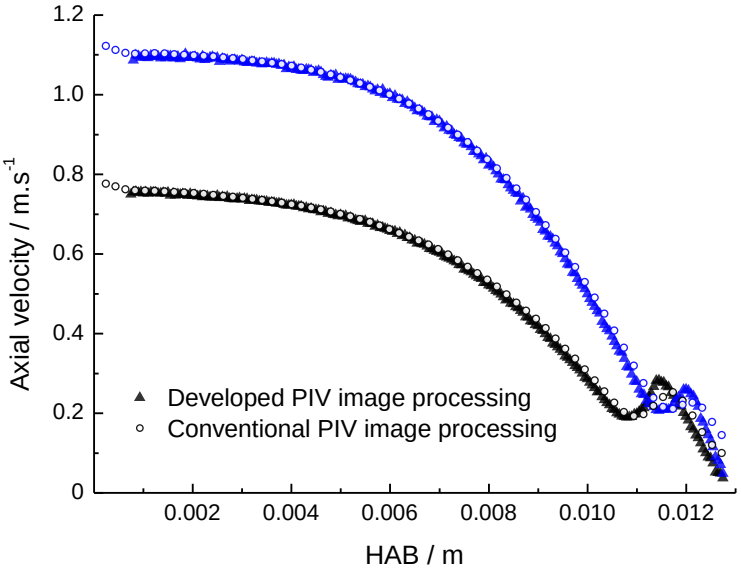

The image processing with an IWS of 32 x 32 pixels results in 64 points axial velocity profiles, while the present methodology allows the determination of the axial velocity profiles with 241 points. It results in a more accurate determination of the reference velocity $S_{u,ref}$.

Figure S2. Evolution of the standard deviation on the determination of the reference axial velocity $S_{u,ref}$ depending on the number of grid points used in the simulation of the axial velocity profile. Simulations are performed with the O_3-submechanism from Jian et al [1].

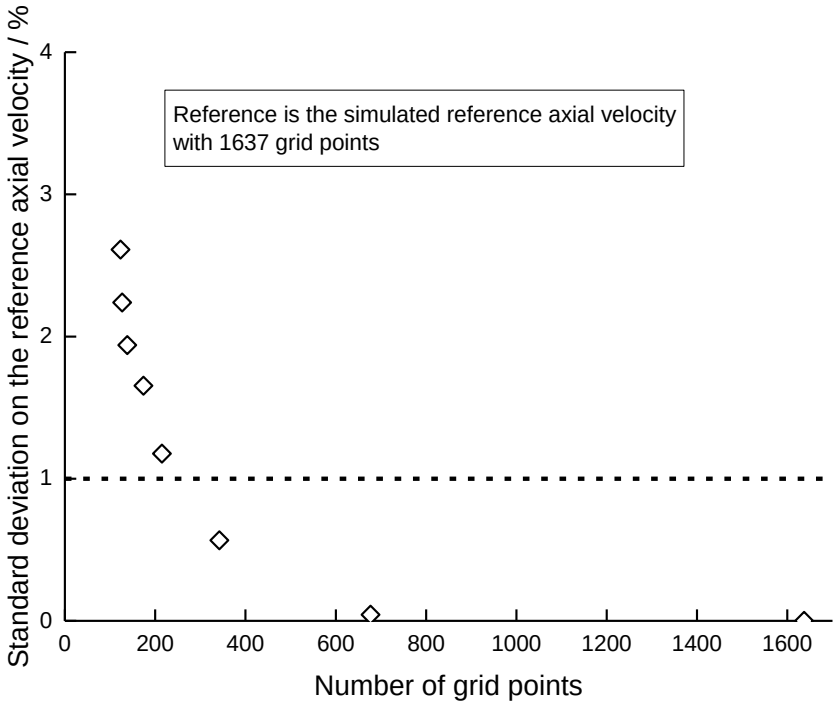

Figure S3. Experimental (open diamonds) PIV measurement of the axial velocity profile for the cool flame at ϕ = 0.5, x_{O3} = 1.5%, and simulated (continuous lines) profiles with different domain sizes *l*. Simulations are performed with the O_3-submechanism from Jian et al [1].

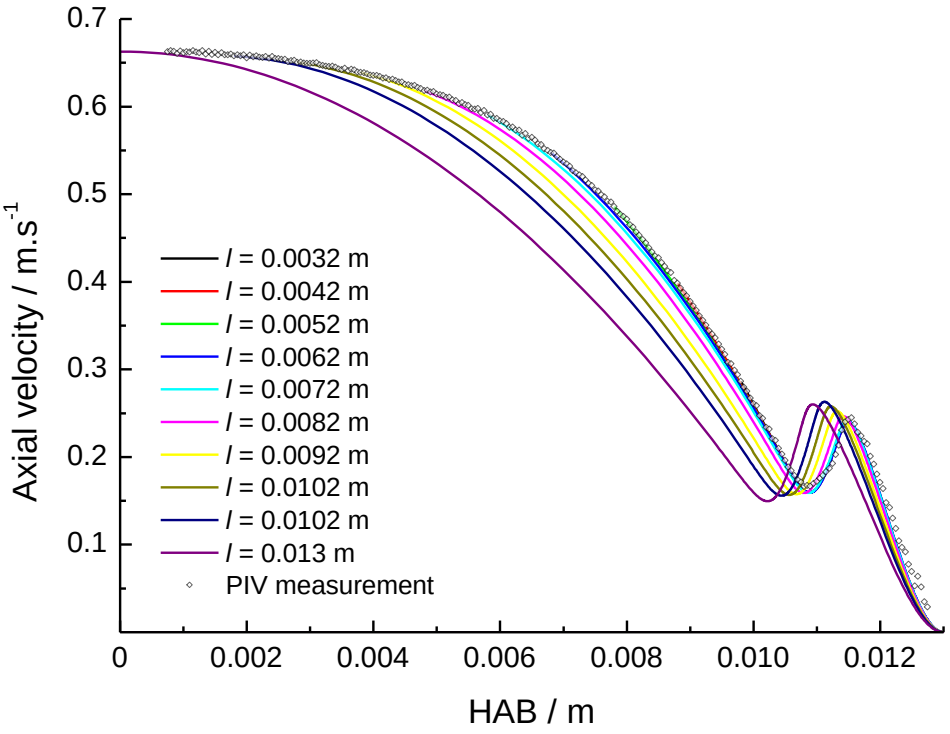

Figure S4. Evolution of the standard deviation on the determination of the value of $S_{u,ref}$ (a) and its position (b) depending on the size of the simulated domain. Simulations are performed with the O_3-submechanism from Jian et al [1].

a)

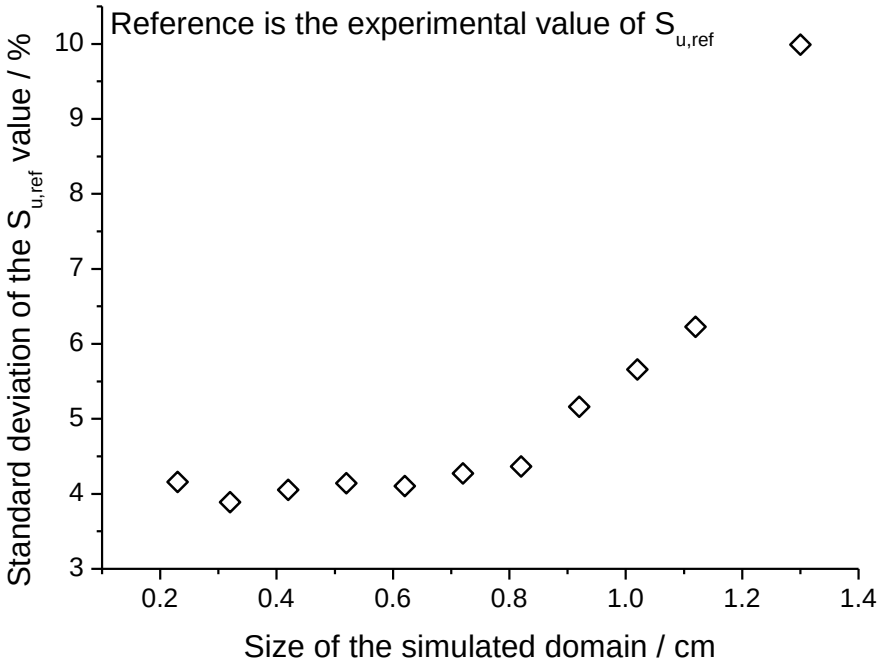

b)

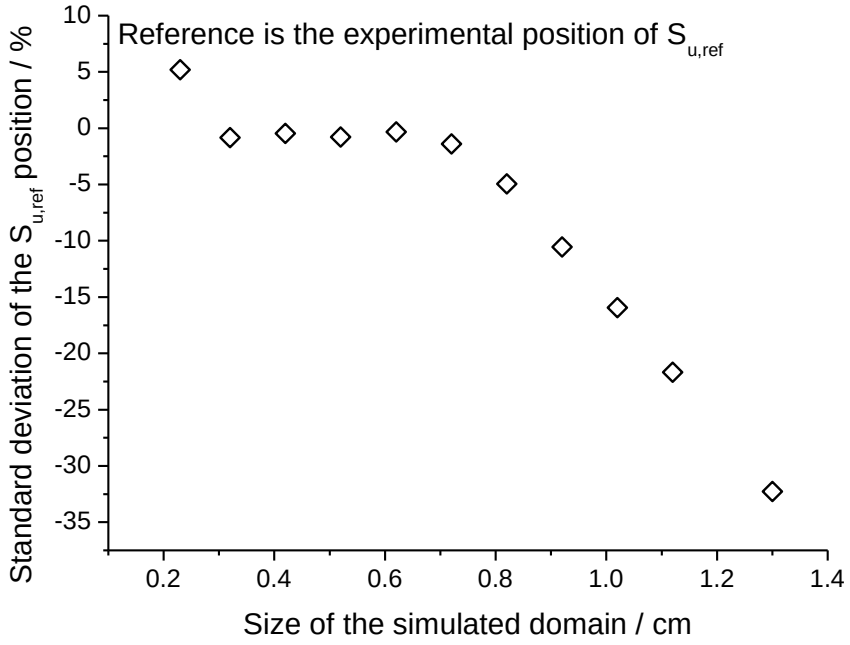

Figure S5. Comparison between experimental axial velocity profiles measured by PIV (□) and simulated ones with different O_3 submechanisms, respectively from Jian et al. [1], Halter et al. [2] and Zhao et al. [3], for the cool flame at $\phi = 0.4$, $x_{O3} = 1.7\%$, at different strain rates.

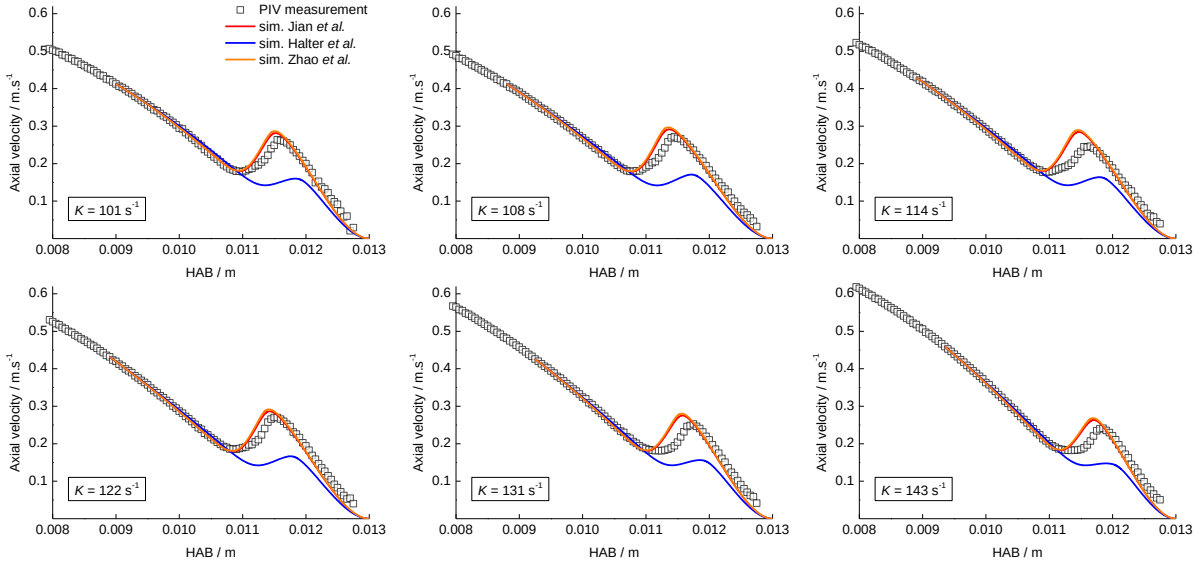

Figure S6. Comparison between experimental axial velocity profiles measured by PIV (□) and simulated ones with different O_3 submechanisms, respectively from Jian et al. [1], Halter et al. [2] and Zhao et al. [3], for the cool flame at $\phi = 0.4$, $x_{O3} = 1.9\%$, at different strain rates.

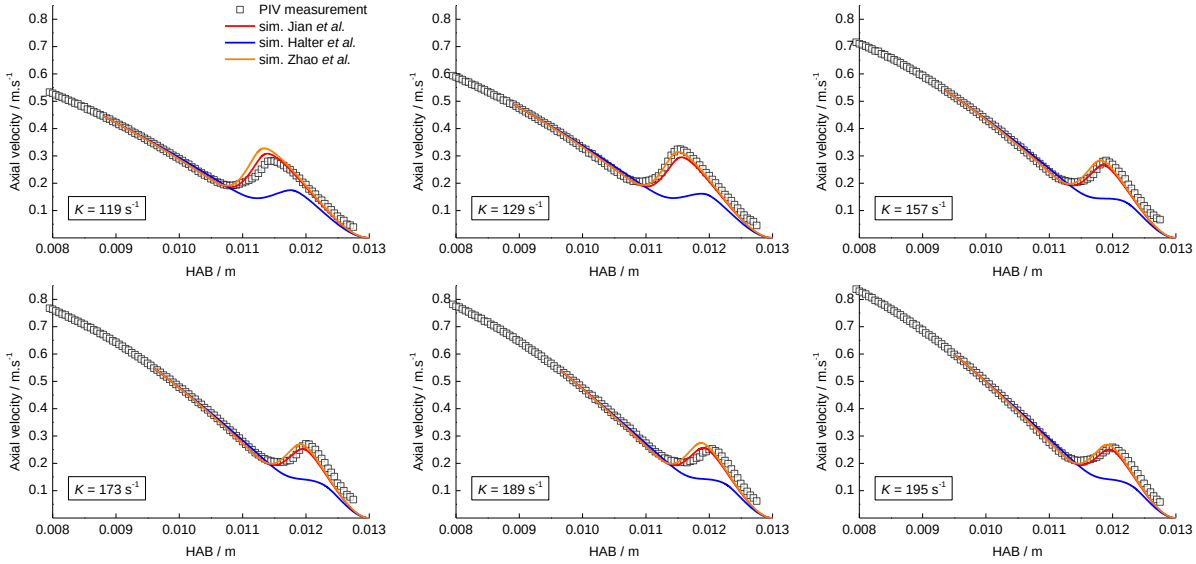

Figure S7. Comparison between experimental axial velocity profiles measured by PIV (□) and simulated ones with different O_3 submechanisms, respectively from Jian et al. [1], Halter et al. [2] and Zhao et al. [3], for the cool flame at $\phi = 0.45$, $x_{O3} = 1.7\%$, at different strain rates.

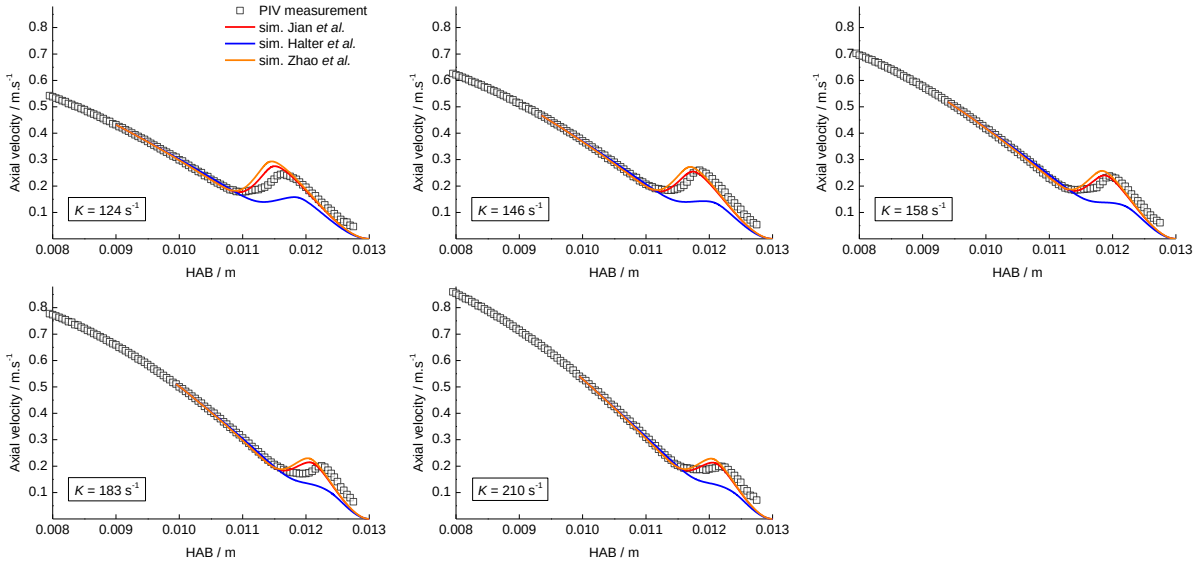

Figure S8. Comparison between simulated axial velocity profiles with O_3-submechanism from Jian et al. [1] and from Jian et al. with O_3+M reactions from Halter et al. [2], for the cool flame at $\phi = 0.5$, $x_{O3} = 1.5\%$ and strain rate of 127 s^{-1}.

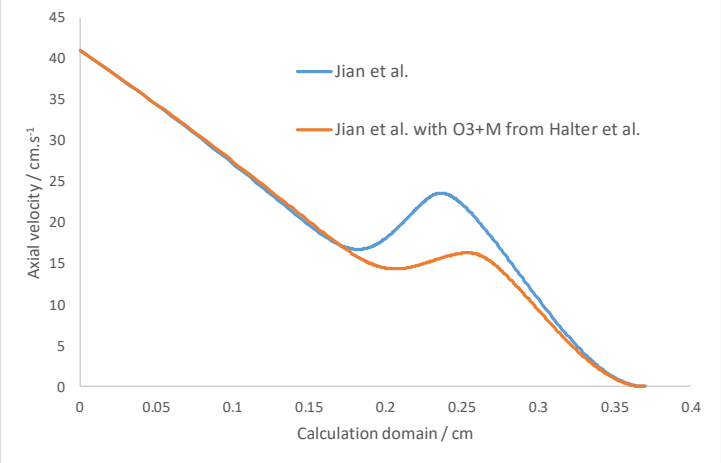

Table T1 : Cool flame conditions

Conditions	**Size of the domain for the axial velocity profiles simulation (**Pre-Mixed Burner Stagnation Flame module) **/ cm**	**Inlet velocity / cm.s^{-1}**	**Imposed radial strain rate / s^{-1}**	**Measured* flame speed / cm.s^{-1}**
ϕ = 0.5 x_{O3} = 1.5% (x_{DME} = 0.144 x_{O2} = 0.841 x_{O3} = 0.015)	0.42	39.9	50.5	16.6
	0.41	40.3	55.6	16.8
	0.4	40.8	59.4	17.0
	0.39	42.5	61.6	17.0
	0.37	41.0	63.7	17.3
ϕ = 0.4 x_{O3} = 1.7% (x_{DME} = 0.119 x_{O2} = 0.864 x_{O3} = 0.017)	0.40	41.3	50.6	17.8
	0.42	41.3	53.9	17.9
	0.41	43.0	56.8	17.7
	0.41	43.2	61.2	18.5
	0.375	42.6	65.3	18.1
	0.365	45.9	71.5	18.2
ϕ = 0.3 x_{O3} = 2.0% (x_{DME} = 0.092 x_{O2} = 0.881 x_{O3} = 0.02)	0.44	41.3	51.5	18.6
	0.445	42.7	53.4	19.4
	0.42	43.1	57.1	18.6
	0.42	44.5	61.2	19.8
	0.42	46.4	61.7	19.9
	0.385	47.7	66.7	19.1
	0.375	49.0	72.8	19.8
	0.325	49.9	82.6	19.0
	0.345	54.7	85.0	19.7
ϕ = 0.4 x_{O3} = 1.9% (x_{DME} = 0.119 x_{O2} = 0.862 x_{O3} = 0.019)	0.42	44.6	59.5	19.1
	0.41	48.9	64.6	20.5
	0.365	54.1	78.5	20.4
	0.34	54.8	86.4	20.4
	0.335	54.0	94.3	20.2
	0.35	59.9	97.6	20.9
ϕ = 0.45 x_{O3} = 1.7% (x_{DME} = 0.132 x_{O2} = 0.851 x_{O3} = 0.017)	0.40	43.2	62.1	17.8
	0.365	46.8	72.8	18.4
	0.36	51.8	79.2	18.5
	0.305	51.1	91.4	18.3
	0.305	54.0	105.3	18.4

*Measured using the numerically assisted non-linear extrapolation method

Table T2. Reactions and rate constant parameters for the three O_3-submechanisms used in the current study

Units: A (cm^3, mole, s), E_a (cal)

Reaction	A	n	E_a
Halter *et al.* [2]			
$O_3 + N_2 \rightarrow O_2 + O + N_2$	4.00E+14	0	22667
$O_2 + O + N_2 \rightarrow O_3 + N_2$	1.60E+14	-0.4	-1391
$O_3 + O_2 \rightarrow O_2 + O_2 + O$	1.54E+14	0	23064
$O_2 + O_2 + O \rightarrow O_3 + O_2$	3.26E+19	-2.1	0
$O_3 + O_3 \rightarrow O_2 + O_3 + O$	4.40E+14	0	23064
$O_2 + O_3 + O \rightarrow O_3 + O_3$	1.67E+15	-0.5	-1391
$O_3 + H \Leftrightarrow O_2 + OH$	8.43E+13	0	934
$O_3 + O \Leftrightarrow O_2 + O_2$	4.82E+12	0	4094
$O_3 + OH \Leftrightarrow O_2 + HO_2$	1.85E+11	0	831
$O_3 + HO_2 \Leftrightarrow O_2 + OH + O_2$	6.02E+09	0	938
$O_3 + H_2O \Leftrightarrow O_2 + H_2O_2$	6.62E+01	0	0
$O_3 + CH_3 \Leftrightarrow O_2 + CH_3O$	3.07E+12	0	417
$O_3 + H \Leftrightarrow O + HO_2$	4.52E+11	0	0
$O_3 + H_2 \Leftrightarrow OH + HO_2$	6.00E+10	0	19840
$O_3 + CH_4 \Leftrightarrow CH_3O + HO_2$	8.13E+10	0	15280
Jian *et al.* [1]			
$O_2 + O + M \Leftrightarrow O_3 + M$	1.00E+19	-2	0
$N_2 = 1.3$; $O_2 = 1.2$; Kr = 1 ; Ar = 1 ; $O_3 = 0$			
$O_2 + O + O_3 \Leftrightarrow O_3 + O_3$	1.00E+23	-3	0
$O_3 + O \Leftrightarrow O_2 + O_2$	1.10E+13	0	4300
$O_3 + H \Leftrightarrow OH + O_2$	8.43E+13	0	934
$O_3 + HO_2 \Leftrightarrow O_2 + O_2 + OH$	5.80E-04	4.57	-1377
$O_3 + OH \Leftrightarrow HO_2 + O_2$	1.20E+05	2.5	800
Zhao *et al.* [3]			
O_3 (+M) $\Leftrightarrow O_2 + O$ (+M)			
Low-Pressure	2.23E+28	-4.37	27297
High-Pressure	1.37E+15	-0.67	25990
Troe Parameters (0.6417 3.91E-04 8680.74 6060.75)			
Ar = 1 ; He = 1.2 ; $N_2 = 1.5$; $H_2 = 3$; $O_2 = 1.5$; $O_3 = 3.75$; O = 6			
$O_3 + O \Leftrightarrow O_2 + O_2$	4.82E+12	0	4094
$O_3 + O \Leftrightarrow O_2$ (sing) + O_2	1.44E+11	0	4094
$O_3 + O \Leftrightarrow O_2 + OH$	8.43E+13	0	934
$O_3 + H \Leftrightarrow O + HO_2$	4.52E+11	0	0
$O_3 + OH \Leftrightarrow O_2 + HO_2$	1.85E+11	0	831
$O_3 + H_2O \Leftrightarrow O_2 + H_2O_2$	6.62E+01	0	0
$O_3 + HO_2 \Leftrightarrow OH + O_2 + O_2$	6.62E+09	0	994
$O_3 + CO \Leftrightarrow O_2 + CO_2$	6.02E+02	0	0
$O_3 + HCO \Leftrightarrow O_2 + H + CO_2$	5.00E+11	0	0
$O_3 + CH_3 \Leftrightarrow CH_3O + O_2$	5.83E+11	0	0

References

[1] J. Jian, H. Hashemi, H. Wu, A.W. Jasper, P. Glarborg, A reaction mechanism for ozone dissociation and reaction with hydrogen at elevated temperature, Fuel. 322 (2022) 124138.

[2] F. Halter, P. Higelin, P. Dagaut, Experimental and Detailed Kinetic Modeling Study of the Effect of Ozone on the Combustion of Methane, Energy Fuels. 25 (2011) 2909–2916.

[3] H. Zhao, X. Yang, Y. Ju, Kinetic studies of ozone assisted low temperature oxidation of dimethyl ether in a flow reactor using molecular-beam mass spectrometry, Combustion and Flame. 173 (2016) 187–194.